Heliyon 10 (2024) e38714

Contents lists available at ScienceDirect

Heliyon

journal homepage: www.cell.com/heliyon

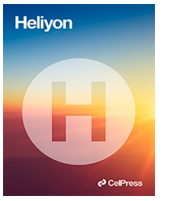

Research article

# Modeling doxorubicin-induced-cardiotoxicity through breast cancer patient specific iPSC-derived heart organoid

Jiye Jang [a,b,c,1], Hyewon Jung [a,b,c,1], Jaekyun Jeong [b,c,1], Junseok Jeon [e], Kyungho Lee [e], Hye Ryoun Jang [e], Jeung-Whan Han [b,c], Jaecheol Lee [a,b,c,d,f,*]

[a] Department of Biopharmaceutical Convergence, Sungkyunkwan University, Suwon, 16419, Republic of Korea
[b] School of Pharmacy, Sungkyunkwan University, Suwon, 16419, Republic of Korea
[c] Epigenome Dynamics Control Research Center (EDCRC), School of Pharmacy, Sungkyunkwan University, Suwon, 16419, Republic of Korea
[d] Biomedical Institute for Convergence at SKKU (BICS), Sungkyunkwan University, Suwon, 16419, Republic of Korea
[e] Division of Nephrology, Department of Medicine, Cell and Gene Therapy Institute, Samsung Medical Center, Sungkyunkwan University, Seoul, Republic of Korea
[f] Department of Biohealth Regulatory Science, Sungkyunkwan University, Suwon, 16419, Republic of Korea

ARTICLE INFO

*Keywords:*
Doxorubicin-induced-cardiotoxicity
Induced pluripotent stem cell
Heart organoid
Disease modeling
Predictive model

ABSTRACT

Heart organoid (HO) technology has successfully overcome the limitations of two-dimensional (2D) disease modeling and drug testing, thereby emerging as a valuable tool in drug discovery for assessing toxicity and efficacy. However, its ability to distinguish drug responses among individuals remain unclear, which is crucial for developing predictive models. We addressed this gap by comparing human induced pluripotent stem cell-derived cardiomyocytes (hiPSC-CMs) with human induced pluripotent stem cell-derived heart organoids (hiPSC-HOs) in the context of doxorubicin-induced cardiotoxicity (DIC). For this study, we utilized hiPSCs generated from breast cancer patients who had previously been treated with doxorubicin. By comparing groups with and without DIC, we examined various parameters, including cell viability, mRNA expression, protein expression and electrophysiological variations. The results of our analysis revealed significant differences between these groups, providing insights into hiPSC-HOs as a potential platform for testing differences in drug responses among patients.

## 1. Introduction

Organoids have been widely used to assess the toxicity and efficacy of drugs, as they exhibit clinical phenotypes that closely mimic physiological tissue responses. These characteristics make them a promising platform for drug testing [1]. However, it remains challenging to clearly elucidate individual differences in drug responses. Therefore, it is important to develop models that address these limitations.

In this study, we investigated the variability in doxorubicin-induced cardiotoxicity (DIC) at the organoid level in individual patients. Doxorubicin, a potent anthracycline chemotherapeutic agent, has demonstrated efficacy in various cancer types, primarily through the inhibition of topoisomerase II (Top2) enzymes [2]. Nevertheless, in certain patients, it is associated with cumulative and

* Corresponding author. Department of Biopharmaceutical Convergence, Sungkyunkwan University, Suwon, 16419, Republic of Korea.
*E-mail address:* jaecheol@skku.edu (J. Lee).
[1] These authors contributed equally to this work.

https://doi.org/10.1016/j.heliyon.2024.e38714
Received 29 April 2024; Received in revised form 26 September 2024; Accepted 27 September 2024
Available online 28 September 2024

dose-dependent cardiotoxicity. DIC is primarily driven by increased oxidative stress and high rates of apoptosis in cardiomyocytes, with contributing factors including free radical generation, mitochondrial dysfunction, and disruption of calcium ion ($Ca^{2+}$) homeostasis [3]. The overall mechanisms of DIC involve increased reactive oxygen species (ROS) production, lipid peroxidation, impaired mitochondrial function, and $Ca^{2+}$ ion imbalance, ultimately leading to apoptosis in cardiomyocytes.

The risk of DIC is significant even at relatively low cumulative doses of doxorubicin (200–250 mg/$m^2$), with an incidence rate between 7.7 % and 8.8 % [4]. Furthermore, DIC is associated with severe adverse effects, including increased left ventricular wall stress, reduced left ventricular ejection fraction, arrhythmias, and congestive heart failure [5]. These side effects are particularly concerning because they are often irreversible. Therefore, it is crucial to predict the possibility of DIC prior to doxorubicin administration [6,7].

To prevent these side effects, preclinical models of cardiotoxicity, particularly approaches utilizing human induced pluripotent stem cell-derived cardiomyocytes (hiPSC-CMs) are becoming increasingly important. Previous studies on DIC have employed breast cancer patient-specific hiPSC-CMs, revealing outcomes such as reduced cell viability, mitochondrial and metabolic dysfunction, impaired calcium handling, decreased antioxidant pathway activity, and increased ROS production [5]. While earlier research focused on the direct effects of doxorubicin on cardiomyocytes, recent studies have demonstrated that various cell types in the heart can also be affected by doxorubicin. For example, doxorubicin-induced damage to the endothelial cells can reduce the release of key endothelial factors and induce apoptosis, thereby promoting the development and progression of cardiomyopathy. However, 2D models cannot reproduce the diverse cellular composition of the heart and its interactions with the extracellular matrix (ECM), making it difficult to accurately assess the clinical impact of doxorubicin [8].

To overcome these limitations, DIC modeling using three-dimensional (3D) systems has been demonstrated as a more effective approach. Considering that non-cardiomyocytes account for more than 60 % of adult human heart tissue, organoid can provide a valuable model to study the interactions among cardiomyocytes as well as between cardiomyocytes and non-cardiomyocytes. Therefore, Using DIC as an example, we propose that 3D organoid models are promising for evaluating drug toxicity and can provide insights into drug responses across various tissue cell types [9,10].

Here, we generated heart organoids derived from breast cancer patients who developed DIC and those who did not, to explore the potential of replicating individual patient drug responses. We also discuss the feasibility of using human induced pluripotent stem cell-derived heart organoid (hiPSC-HOs) for drug screening and their utility as a predictive model.

## 2. Materials and methods

### 2.1. Human-induced pluripotent cell culture

DOX and DOXTOX human induced pluripotent stem cells (hiPSCs) were obtained from Greenstone Biosciences, Inc. (CA, USA). The hiPSC lines used in the experiment were the same as the DOX4(65FSDNC2) and DOXTOX3(51FSDNC18) lines described in a previous study [5]. Healthy normal control hiPSCs were generated at the Cell and Gene Therapy Institute, Samsung Medical Center. The hiPSCs were cultured in E8 medium (A1517001, Gibco, MA, Waltham, USA) on a 1:400 Matrigel basement membrane matrix (354234, Corning, Arizona, USA) and passaged every 3–4 days using 0.5 mM EDTA (LS015-02, Welgene, Kyungsan, Gyeongsangbuk-do, Korea). All cultures were maintained in 2 mL of medium per well in 6-well cell culture plates (30006, SPL, Pocheon, Gyeonggi-do, Korea) [11]. Regular testing for *Mycoplasma* contamination was conducted using the e-Myco Mycoplasma PCR Detection Kit (25235, iNtRON, Seongnam, Gyeonggi-do, Korea).

### 2.2. The hiPSC-derived heart organoid generation

To generate heart organoids, embryoid bodies (EBs) were first formed by dissociating hiPSCs into single cells using 0.5 mM EDTA. The cells were then centrifuged at 300 g for 5 min and resuspended in E8 medium containing 10 μM of ROCK inhibitor (1293823, BioGems, Westlake Village, CA, USA). Live cells were counted using trypan blue staining (T8154, SIGMA, MS, St. Louis, USA) and the LUNA-II™ Automated Cell Counter (L40002, Logos Biosystems, Anyang, Gyeonggi-do, Korea), then seeded at 10,000 cells/well in V-bottom ultra-low attachment 96-well plates (MS-9096VZ, Shimadz, Kyoto, Japan) on day 2, with a volume of 100 μL per well. The plates were centrifuged at 500 g for 3 min and placed in an incubator at 37 °C and 5 % $CO_2$. After 24 h (day 1), 50 μL of media was carefully removed from each well and 200 μL of fresh E8 medium was added, thus a total volume of 250 μL/well was obtained. The plates were returned to the incubator for 24 h. On day 0, 166 μL (~2/3 of the total well volume) of media was aspirated from each well and 166 μL of RPMI 1640 (LM011-01, Welgene)/B-27 minus insulin (A1895601, Gibco) containing CHIR99021 (4423, Tocris, Bristol Avonmouth, England) was added to a final concentration of 6 μM/well. On day 1, 166 μL of the medium was removed and replaced with fresh RPMI1640/B-27, minus insulin. On day 2, RPMI/B-27 minus insulin containing the Wnt inhibitor endo IWR-1 (3532, Tocris), was added to a final concentration of 5 μM IWR-1 and the samples were incubated for 48 h. The medium was changed again on days 4 and 6, and insulin was added to the RPMI 1640/B-27 (17504044, Gibco) mixture on day 6. On day 7, organoids were exposed to a second treatment with 2 μM CHIR99021 for 1 h in RPMI1640/B-27 and the medium was changed every 48 h [12].

### 2.3. Cardiomyocyte differentiation of hiPSCs

The hiPSCs were split in a ratio of 1:12 using EDTA, as previously described, and cultured for 3–4 days until they reached approximately 80 % confluency. The medium was then changed to RPMI 1640/B-27 minus insulin containing 4–6 μM CHIR99021, and

1 mL of medium was added for the next 2 days. On day 3, the medium was switched to RPMI 1640/B-27 minus insulin containing 5 μM IWR-1. The medium was changed on day 5 and every other day thereafter. On day 9, the medium was replaced with RPMI 1640/B-27 and beating cells were observed. On day 11, the medium was replaced with RPMI 1640 without glucose (LM011-60, Welgene)/B-27 and changed again on day 13. On day 15, the medium was replaced with RPMI 1640/B-27 [13,14].

### 2.4. Quantitative real-time PCR

To analyze gene expression, cardiomyocytes were dissociated with TrypLE Select (A1217701, Gibco) for 10 min at 37 °C and 5 % $CO_2$, then triturated, diluted in phosphate-buffered saline (PBS; LB001-02, Welgene), and centrifuged at 300 g for 3 min. The medium was aspirated and the RNA was isolated using the easy-BLUE Total RNA Extraction kit (iNtRON) and stored at −80 °C. The cDNA was synthesized using 2× PCR Master Mix Solution (i-Taq, iNtRON), and real-time PCR was performed. All PCR reactions were conducted in biological duplicate, normalized to the 18S rRNA endogenous control gene, and assessed using the comparative Ct method (Table S1). [15].

### 2.5. Organoid immunofluorescent staining

The hiPSC-HOs were transferred to 1.7 mL microcentrifuge tubes (10721433, Axygen, Arizona, USA) using a cut 200 μL pipette tip to avoid disruption to the organoids and washed with PBS. HOs were fixed in 4 % paraformaldehyde for 30 min at room temperature (RT). The fixed cells were washed with PBS, washed once with 50 % methanol in PBS, 80 % ethanol in deionized water, and finally with 100 % methanol. This process was repeated in reverse order. The HOs were subsequently permeabilized in PBS containing 0.2 % Triton X-100 and 20 % dimethyl sulfoxide (DMSO) at RT for 1 h and blocked in PBS containing 0.2 % Triton X-100, 6 % donkey serum, and 5 % DMSO at RT for 30 min. HOs were incubated with primary antibodies in PBS containing 0.2 % Tween 20, 3 % donkey serum, and 10 % DMSO at 4 °C overnight. After exposure to the primary antibody, six washes were conducted in PBS with 0.2 % Tween 20 and 10 μg/mL heparin. The HOs were then incubated with secondary antibodies and Hoechst in PBS with 0.2 % Tween 20, 3 % donkey serum, and 10 % DMSO in a thermal mixer at 300 rpm and at 4 °C for 1 h in the dark. The stained HOs were washed six times in PBS with 0.2 % Tween 20 and 10 μg/mL heparin before being cleared on a glass-bottom cell culture dish (801001, NEST, Wuxi, China) using the CytoVista 3D Cell Culture Clearing Reagent (V11315, Invitrogen, MA, Waltham, USA).

#### 2.5.1. Confocal microscopy

Sample images were captured using a confocal laser scanning microscope (Leica Stellaris 5). Image analysis was performed using LAS X software. For cell quantification of the organoids, TNNT2-positive cells were counted and normalized to the target cell marker of interest.

### 2.6. Doxorubicin treatment

Cardiomyocytes were dissociated on differentiation day 19 using TrypLE Select for 10 min at 37 °C, and 5 % $CO_2$, centrifuged at 1300 rpm for 6 min, and filtered through a 100 μm cell strainer. The live cells were stained with trypan blue and counted using the LUNA-II Automated Cell Counter. Cells were seeded at a density of 10,000 cells/well in 96-well cell culture plates (30096, SPL) in RPMI 1640/B-27. Doxorubicin hydrochloride (D1515, Sigma-Aldrich) was resuspended in 10 mM DMSO (D1370.1000, Duchefa Biochemie, RV Haarlem, Netherlands). For cell treatments using day 30 hiPSC-CMs, cells were treated with doxorubicin ($10^{-1}$–$10^{-6}$ μM) diluted in RPMI 1640/B-27 for 3 days. hiPSC-HOs were treated on day 15 with doxorubicin ($10^{-1}$–$10^{-6}$ μM) diluted in RPMI 1640/B-27 for 1–6 days.

### 2.7. Viability assay for cardiomyocytes and heart organoids

DMSO was used as a control for cardiomyocytes. The hiPSC-CMs exposed to doxorubicin were washed with PBS and incubated in PrestoBlue cell viability reagent (A-13261, Invitrogen) diluted in RPMI 1640 medium supplemented with B-27 at 37 °C and 5 % $CO_2$ for 3 h. The fluorescence was measured using Cytation 5 at excitation and emission wavelengths of 570 and 600 nm, respectively. Data were analyzed using the Prism 8 software (GraphPad, San Diego, CA, USA) following standard concentration–response guidelines. For heart organoids, hiPSC-HOs exposed to doxorubicin were washed with PBS and incubated in PrestoBlue cell viability reagent (A-13261, Invitrogen) diluted in Roswell Park Memorial Institute (RPMI) 1640 medium supplemented with B-27 at 37 °C and 5 % $CO_2$ for 12 h. The fluorescence was quantified at 560/590 nm (excitation/emission). Data were analyzed using the Prism 8 software (GraphPad) following standard concentration–response guidelines [16].

### 2.8. Microelectrode array

Before plating the hiPSC-HOs, the 1:100 Matrigel basement membrane matrix was pipetted onto the array and left at 37 °C and 5 % $CO_2$ for 3 h. Matrigel was then aspirated, and HOs were carefully placed on the node in 20 μL of RPMI 1640/B-27 containing 10 μM of a ROCK inhibitor, then left at 37 °C and 5 % $CO_2$ for 10 h. The next day, 500 μL of RPMI 1640/B-27 was added and the media was changed every 48 h until organoids were ready for analysis. Field potentials (FPs) of hiPSC-HOs were recorded using a microelectrode array system (Axion Biosystems, Atlanta, GA, USA) using the Axis Navigator software. Effects of the beat period were assessed in the

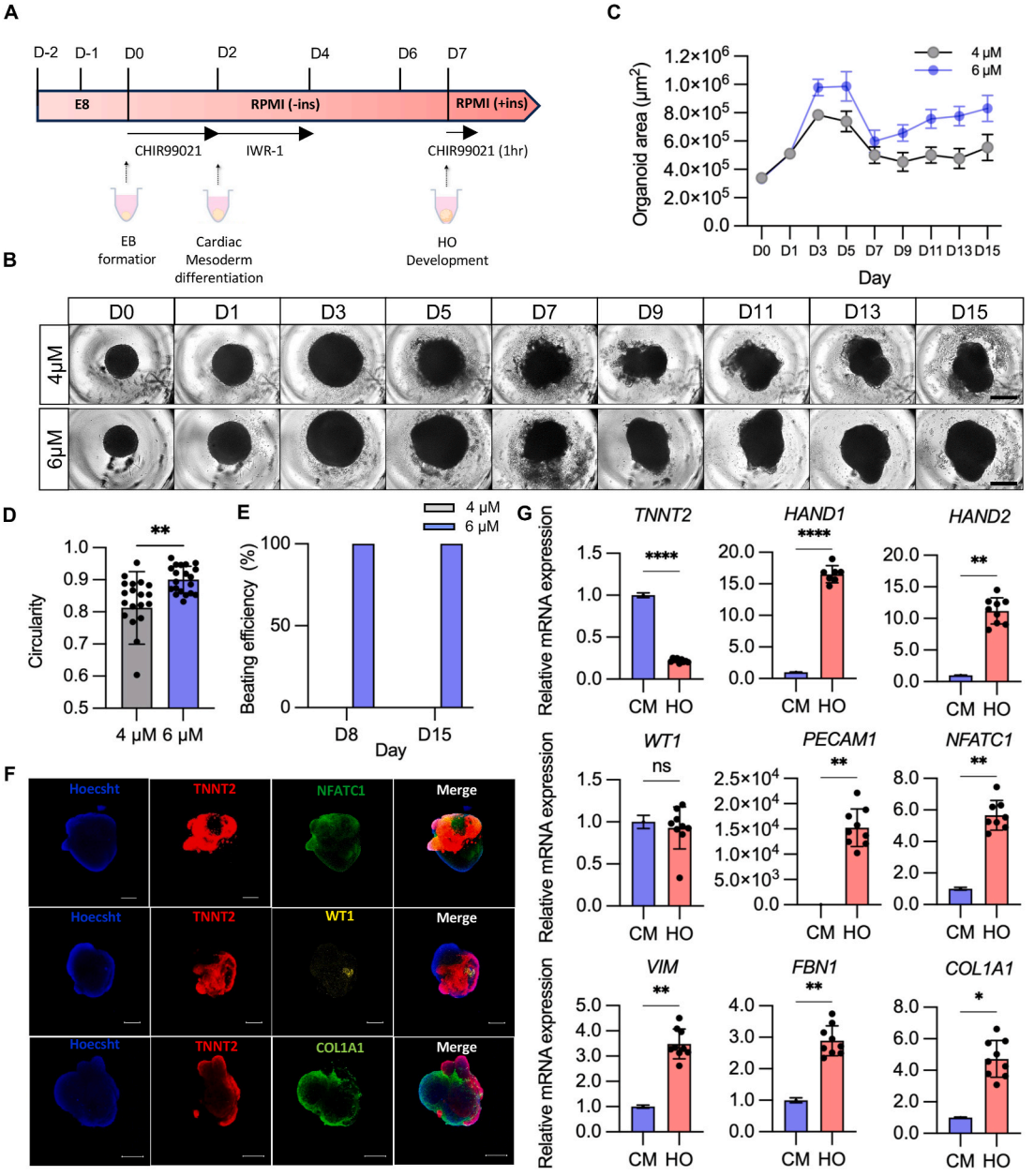


**Fig. 1. Generation of normal hiPSC derived 3D-HOs**

A. Schematic diagram illustrating the protocol used for the differentiation of 3D-HOs from embryoid bodies.

B. Phase-contrast images showing the development of 3D-HOs over 15 days of differentiation at various CHIR99021 concentrations. Scale bar = 500 μm

C. Average area of developing 3D-HOs over 15 days of differentiation at various CHIR99021 concentrations. n = 30. Mean ± SD.

D. Circularity of organoids on day 15 with various CHIR99021 concentrations. n = 30. Mean ± SD.

E. Percentage of beating organoids on days 8 and 15 with various CHIR99021 concentrations. n = 30.

F. Immunofluorescence analysis of endocardial cells (NFATC1, green), epicardial cells (WT1, yellow), and fibroblasts (COL1A1, green) counter-stained with Hoechst (blue). Scale bar = 200 μm

G. Gene expression analysis was performed on both 2D-CMs (n = 1) and 3D-HOs (n = 6–9), including the first and second heart field markers (HAND1 and HAND2) and cardiac-specific cell type populations in 3D-HOs, including cardiomyocytes (TNNT2), endocardial cells (NFATC1), epicardial cells (WT1), endothelium (PECAM1), and fibroblasts (VIM, COL1A1, and FBN1). Mean ± SD. Cardiomyocyte, CM; Heart organoid, HO; p value: *t*-test *($p < 0.05$); **($p < 0.01$); ***($p < 0.001$); ns: not significant ($p > 0.05$).

presence and absence of doxorubicin [17].

## 3. Results

### 3.1. Generation of induced pluripotent stem cell-derived 3D heart organoids and comparison with 2D cardiomyocytes

To characterize DIC, we generated both hiPSC-CMs (2D-CMs) and hiPSC-HOs (3D-HOs) [5,12]. Briefly, hiPSCs were cultured in V-bottom ultra-low attachment plates to form EB spheroids, which were subsequently induced into the mesodermal and cardiac lineages using CHIR99021 (a GSK3 inhibitor) and endo-IWR1 (Fig. 1a). Next, 3D-HOs were generated using various concentrations of CHIR99021 to determine its optimal condition of CHIR99021 [18]. The 6 μM CHIR99021 group exhibited slightly larger organoid size during the cardio-mesodermal differentiation stage, although no significant differences were observed during the EB stage (Fig. 1b and c). Moreover, the 6 μM CHIR99021 group demonstrated consistent morphological stability and well-defined boundary structures, as quantified by circularity analysis (Fig. 1b and d). Additionally, the proportion of beating organoids was evaluated with no beating

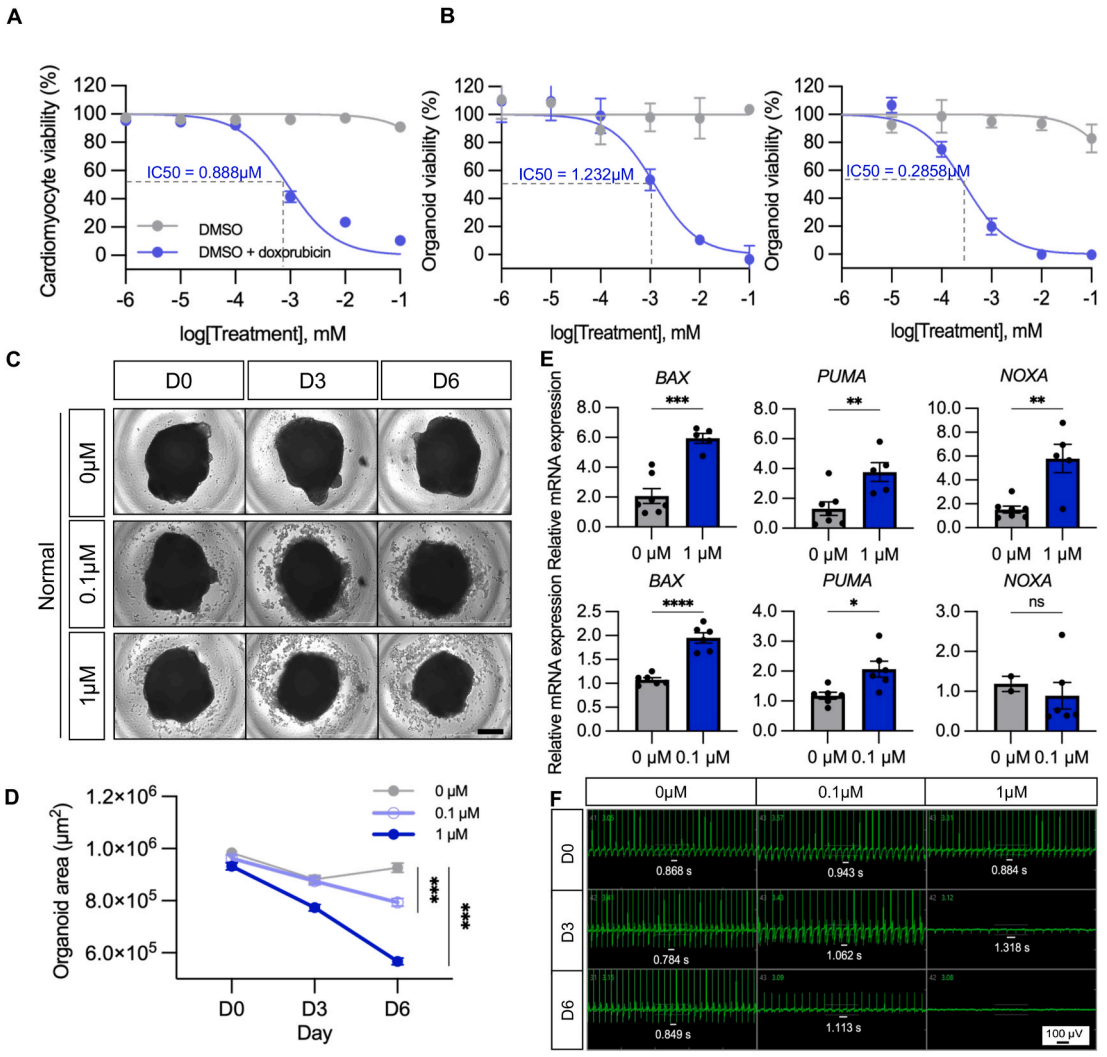


**Fig. 2. Doxorubicin-induced cardiotoxicity in normal hiPSC-derived 3D-HOs**

A. Effect of doxorubicin (3 days) on 2D-CMs viability using the PrestoBlue assay. n = 6. Mean ± SD.

B. Effect of doxorubicin (left: 3 days, right: 6 days) on 3D-HOs viability using the PrestoBlue assay. n = 10. Mean ± SD.

C. Phase contrast images of 3D-HOs after treatment with specific concentrations of doxorubicin for 6 days. Scale bar = 500 μm.

D. Average area of 3D-HOs after treatment with specific concentrations of doxorubicin for 6 days. n = 18~30. Mean ± SD.

E. Gene expression analysis of apoptosis markers in 3D-HOs with or without 1 μM for 3 days (top) and 0.1 μM for 6 days (bottom) of doxorubicin. *p value: *t*-test *($p < 0.05$); **($p < 0.01$); ***($p < 0.001$); ns: not significant ($p > 0.05$).

F. Electrophysiological analysis of 3D-HOs in response to treatment with specific concentrations of doxorubicin for 3 days on an MEA system. White line represents beat period (s).

observed in the 4 μM group, while all organoids in the 6 μM group displayed beating activity (Fig. 1e). The comprehensive analysis of circularity measurements and phenotypic imaging revealed that treatment with 6 μM CHIR99021 significantly improved cohesiveness and enhanced the efficiency of generating larger beating organoids compared to the 4 μM treatment. Immunofluorescence staining confirmed the presence of cardiomyocytes (TNNT2) and non-cardiomyocytes (WT1, NFATC1, and CO1A1) within the 3D-HOs (Fig. 1f) [12,19–23]. Gene expression analysis was also conducted to compare the characteristics of 2D-CMs and 3D-HOs. Reverse

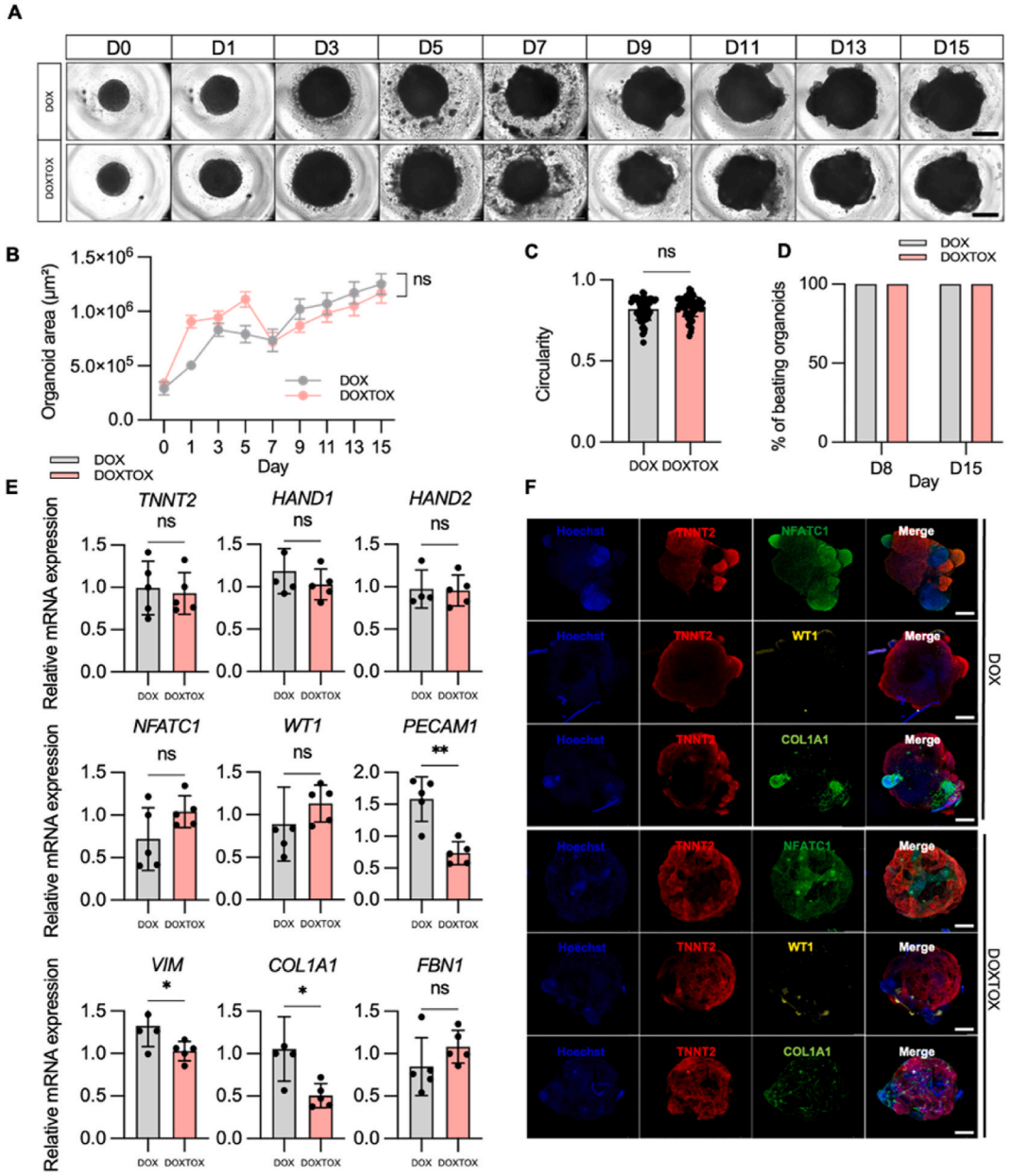


**Fig. 3.** Generation of Patient specific hiPSC-derived 3D-HOs

A. Phase-contrast images of developing DOX and DOXTOX-HOs after 15 days of differentiation. Scale bar = 500 μm

B. Average area for developing DOX and DOXTOX-HOs over 15 days of differentiation. n = 60 organoids. Mean ± SD.

C. Circularity of DOX and DOXTOX-HOs on day 15. n = 60. Mean ± SD.

D. Percentage of beating efficiency on day 8 and 15. n = 60. Mean ± SD.

E. Gene expression analysis of the first and second heart field markers (HAND1 and HAND2) and cardiac-specific cell type populations in DOX and DOXTOX-HOs, including cardiomyocytes (TNNT2) and endocardial cells (NFATC1). Epicardial cells (WT1), endothelium (PECAM1), and fibroblasts (VIM, COL1A1, and FBN1) on day 15. n = 5. Mean ± SD. *p value: *t*-test *($p < 0.05$); **($p < 0.01$); ***($p < 0.001$); ns: not significant ($p > 0.05$).

F. Immunofluorescence analysis of multiple cell types (NFATC1; green), epicardial cells (WT1; yellow), and fibroblasts (COL1A1; green) counter-stained with Hoechst stain (blue). Scale bar = 200 μm.

transcriptase-quantitative polymerase chain reaction (RT-qPCR) results indicated that although TNNT2 expression was lower in the 3D-HOs than in the 2D-CMs, the 3D-HOs exhibited the presence of various cardiac cell types. Markers for the non-cardiomyocytes (first/second heart fields (HAND1 and HAND2) [24,25], endocardial cells (NFATC1), endothelial cells (PECAM1), and fibroblasts (VIM, COL1A1, and FBN1)) [26–28] were expressed at higher levels in 3D-HOs than in 2D-CMs (Fig. 1g) [12]. These results indicate that although 3D-HOs exhibit lower expression of cardiomyocyte markers compared to 2D-CMs, they express markers for a broader range of cardiac cell types, suggesting the presence of a more diverse cellular composition within the 3D-HOs.

### 3.2. The hiPSC-derived heart organoids can recapitulate doxorubicin-induced cardiotoxicity

We conducted a comprehensive evaluation of cell viability, gene expression, and functional parameters to confirm DIC in 3D-HOs [29–31]. First, both normal 2D-CMs and 3D-HOs were treated with doxorubicin for 3 days. A dose-dependent reduction in cell viability was observed in both the 2D and 3D models compared to vehicle-treated controls. However, a difference in the $IC_{50}$ values between the 2D model (0.888 μM) and the 3D (1.232 μM) model was observed (Fig. 2a and b). To further assess the appropriateness of doxorubicin treatment, an additional 6 day treatment experiment was conducted, revealing a lower $IC_{50}$ value (0.2858 μM). Morphological changes, including surface structure collapse and increased debris, were observed after 3 days of treatment with 1 μM doxorubicin (Fig. 2c) [31]. Additionally, after six days of treatment with 0.1 μM and 1 μM doxorubicin, area of the 3D-HOs decreased by approximately 20 % (Fig. 2d). Moreover, RT-qPCR analysis demonstrated a significant upregulation of apoptotic marker genes, including BAX, PUMA, and NOXA, following 3 days of treatment with 1 μM doxorubicin (Fig. 2e, top) [31–33]. However, when treated with 0.1 μM doxorubicin for 6 days, only specific apoptosis markers, such as BAX, were observed, with no notable trend (Fig. 2e, bottom). These findings demonstrate the utility of 3D-HOs as a model for DIC under appropriate concentration and duration conditions. The functional aspects of 3D-HOs were assessed using multi-electrode array (MEA) analysis [34–36], which showed an increase in beating intervals following doxorubicin treatment, with more pronounced effects at higher concentrations (Fig. 2f). We showed that 3D-HOs successfully recapitulated DIC in terms of both cell death and functional phenotypes during doxorubicin treatment.

### 3.3. Generation of patient-specific hiPSC-derived 3D heart organoids

To validate the ability of the 3D-HO model to distinguish between the differences in DIC within patients, we differentiated 3D-HOs using two distinct hiPSC lines. We generated 3D-HOs from breast cancer patient-derived hiPSC without DIC (referred to as "DOX") and with DIC (referred to as "DOXTOX") [5]. While investigating the differences between DOX-HOs and DOXTOX-HOs, we found that organoid size and circularity were similar throughout the differentiation process. (Fig. 3a, b, and 3c). Additionally, there was no significant difference in the proportion of beating organoids between the differentiated DOX-HOs and DOXTOX-HOs (Fig. 3d, Fig. S1). RT-qPCR analysis further revealed that the expression of cardiomyocyte and non-cardiomyocyte markers was comparable between the DOX-HOs and DOXTOX-HOs. The expression of the endothelial marker (PECAM1) was reduced in DOXTOX-HOs, while no evident trend was observed for the fibroblast markers (VIM, COL1A1, and FBN1) (Fig. 3e). Whole-mount immunostaining analysis of the 3D-HOs demonstrated the presence of various cardiac cell types that expressed diverse markers such as TNNT2, NFATC1, COL1A1, and WT1 in both DOX-HOs- and DOXTOX-HOs (Fig. 3f). Thus, no significant differences were observed in the 3D heart organoid differentiation between the DOX-HOs and DOXTOX-HOs under normal conditions.

### 3.4. Distinguishing patient-specific responsiveness to doxorubicin using hiPSC-derived 3D heart organoids

Based on our previous results, DOX-HOs and DOXTOX-HOs showed no significant differences in differentiation under normal conditions, we hypothesized that these models could be used to distinguish specific responses to DIC. We then examined differences in cell viability, gene expression, and physiological function between the DOX and DOXTOX groups upon doxorubicin exposure.

First, we assessed the cell viability in DOX- and DOXTOX-derived 2D-CMs and 3D-HOs. In both models, the DOXTOX line exhibited significantly lower $IC_{50}$ values after 3 days of doxorubicin treatment compared to the DOX line (13.67 μM for DOX-CMs and 0.7704 μM for DOXTOX-CMs; 11.96 μM for DOX-HOs and 1.494 μM for DOXTOX-HOs) (Fig. 4a and b left). However, no significant differences were observed between 3D-HOs after six days of doxorubicin treatment (Fig. 4b, right). Considering the lower $IC_{50}$ values observed after three days of doxorubicin treatment, we suggest that specific conditions can induce excessive toxicity in DOXTOX patients. Our results emphasize the importance of treatment duration in distinguishing differential responsiveness among patients. Next, we observed structural changes, including surface collapse and a decrease in organoid size, in both DOX-HOs and DOXTOX-HOs during doxorubicin treatment (Fig. 4c). A reduction in the surrounding area of the HOs were observed for both the DOX-HOs and DOXTOX-HOs (Fig. 4d). Additionally, gene expression analysis revealed an increase in the expression of apoptotic markers in both DOX-HOs and DOXTOX-HOs following doxorubicin treatment. As previously reported, we first confirmed the differences in apoptotic markers between DOX-CMs and DOXTOX-CMs after doxorubicin treatment [5]. A significant increase in the expression of BAX, NOXA, and PUMA was observed in DOXTOX-CMs treated with 1 μM doxorubicin for three days (Fig. S2). Similarly, a distinct difference in gene expression was identified between DOX-HOs and DOXTOX-HOs following three days of treatment with 1 μM doxorubicin (Fig. 4e). However, similar to the results of the $IC_{50}$ measurements, no significant differences were observed in apoptotic gene markers between DOX-HOs and DOXTOX-HOs treated with 0.1 μM doxorubicin for 6 days. These findings emphasize the importance of appropriate drug treatment concentrations and durations for distinguishing patient-specific drug responses between DOX-HOs and DOXTOX-HOs under different exposure conditions. We also observed interesting results when comparing the fold-changes in apoptotic markers before and after doxorubicin treatment between the 2D-CMs and 3D-HOs (Fig. S3). Changes in BAX expression were more pronounced in the

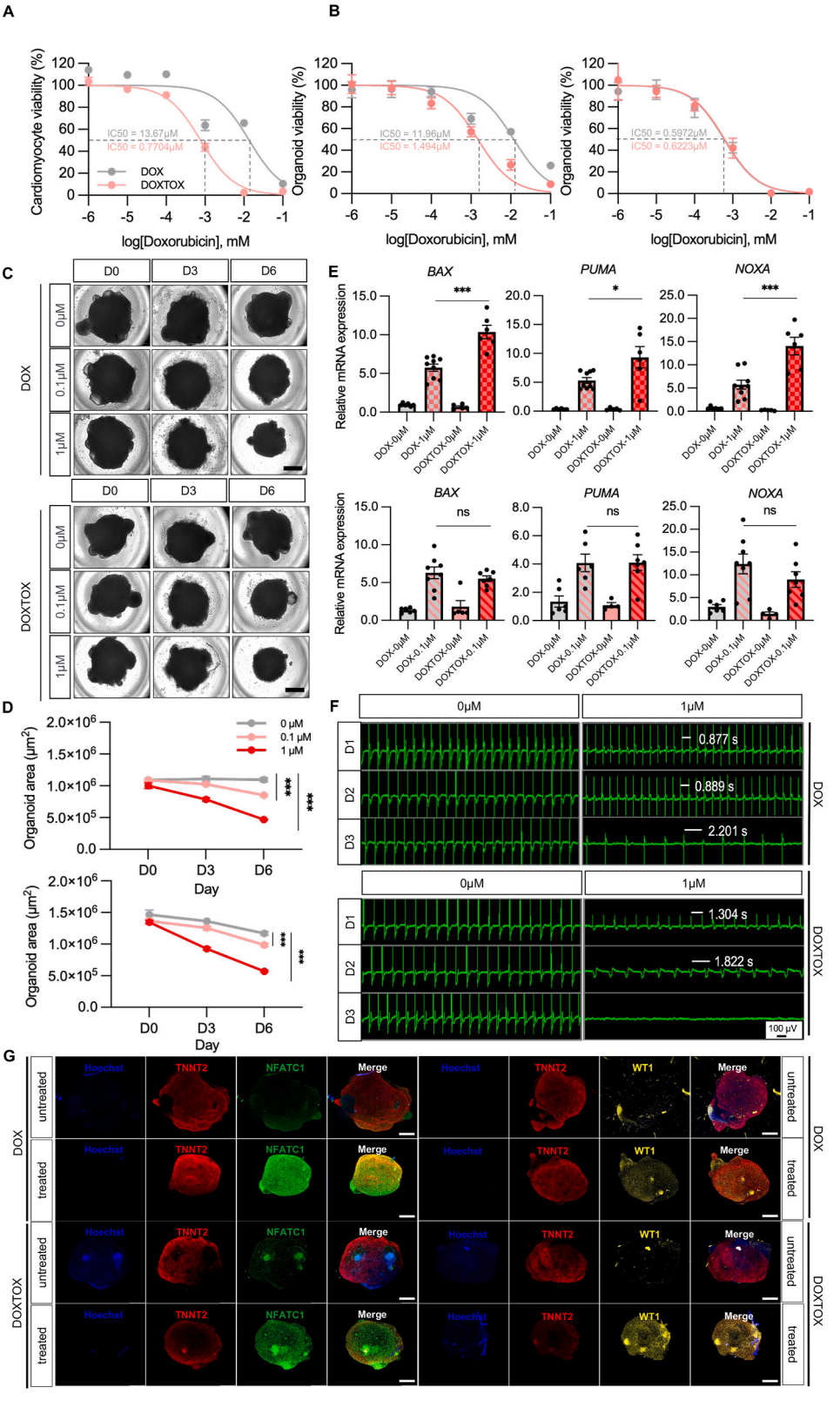


*(caption on next page)*

**Fig. 4.** Doxorubicin-induced cardiotoxicity in patient-specific hiPSC-derived 3D-HOs
A. Effect of doxorubicin (3 days) on DOX and DOXTOX-CM viability using the PrestoBlue assay. n = 6. Mean ± SD.
B. Effect of doxorubicin (left: 3 days, right: 6 days) on DOX and DOXTOX-HO viability using the PrestoBlue assay. n = 10. Mean ± SD.
C. Phase-contrast images after treatment with the specified concentrations of doxorubicin for 6 days. Scale bar = 500 μm.
D. Average area of DOX and DOXTOX-HOs after treatment with specified concentrations of doxorubicin for six days. n = 6∼10. Mean ± SD.
E. Gene expression analysis of apoptosis markers in DOX and DOXTOX-HOs with 1 μM for 3 days (top) and 0.1 μM for 6 days (bottom) doxorubicin, n = 6∼9. Mean ± SD. *$p$-value: $t$-test *($p < 0.05$); **($p < 0.01$); ***($p < 0.001$); ns: not significant ($p > 0.05$).
F. Electrophysiological analysis of DOX and DOXTOX-HOs after treatment with specified concentrations of doxorubicin for 3 days in an MEA system. n = 8. Mean ± SD. White line represents beat period (seconds).
G. Immunofluorescence analysis of multiple cell types (NFATC1; green), epicardial cells (WT1; yellow), and fibroblasts (COL1A1; green) counterstained with Hoechst stain (blue). Scale bar = 200 μm.

3D-HOs than in the 2D-CMs, while PUMA expression in the 2D-CMs was more sensitive to doxorubicin treatment than in the 3D-HOs. However, NOXA expression exhibited a different pattern. These varying patterns of apoptotic marker expression suggest that the 2D-CMs and 3D-HOs respond differently to doxorubicin treatment.

Finally, MEA was performed to investigate the functional differences between DOX-HOs and DOXTOX-HOs after treatment with doxorubicin. The beating period of DOXTOX-HOs progressively increased and eventually stopped after 3 days of doxorubicin treatment. Increase in the beating period was more pronounced for the DOXTOX-HOs (1.304 s on day 1 and 1.822 s on day 2) than for DOX-HOs (0.877 s on day 1 and 0.889 s on day 2) (Fig. 4f). Immunostaining analysis revealed a significant decrease in the cardiomyocyte marker TNNT2 in DOXTOX-HOs after 3 days of treatment with 1 μM doxorubicin. However, expression of endocardial (NFATC1) and epicardial (WT1) markers increased in all DOX and DOXTOX-HOs following doxorubicin treatment (Fig. 4g). Our study highlights the different responses of the DOX-HOs and DOXTOX-HOs following doxorubicin treatment, which is consistent with previous DIC research using 2D-CMs. These differences include lower viability, reduced beating rates, and increased expression of apoptosis-related genes in DOXTOX-HOs after doxorubicin treatment. Moreover, we observed a decrease in the cardiomyocyte area in DOXTOX-HOs, whereas the non-cardiomyocyte area increased in both DOX-HOs and DOXTOX-HOs. Additionally, our findings emphasize the importance of determining the appropriate drug concentration and treatment duration to effectively distinguish drug responses among patients.

## 4. Discussion

Our study demonstrates that 3D-HOs derived from patient-specific hiPSCs can effectively reveal differences in doxorubicin responsiveness. The HO system exhibited reduced cell viability and increased apoptosis following doxorubicin treatment. By optimizing the drug concentration and treatment duration (three days of 1 μM doxorubicin), we successfully induced features associated with doxorubicin-induced cardiotoxicity (DIC) in our hiPSC-HO system. Under these conditions, DOXTOX-HOs displayed increased sensitivity to doxorubicin compared to DOX-HOs, with lower viability, higher expression of apoptosis-related genes, and a more significant reduction in beating rates. These findings suggest that 3D-HOs have the capability to distinguish between the DIC phenotypes observed in patients.

The differential responsiveness between DOX-HOs and DOXTOX-HOs can be attributed to distinct molecular mechanisms within cardiomyocytes, the predominant cell type in the organoids [12,37]. Previous studies have identified significant changes in gene expression profiles in 2D cardiomyocytes (2D-CMs) between the DOX and DOXTOX groups, particularly in genes associated with increased reactive oxygen species (ROS) production and oxidative stress [5]. These findings are applicable to cardiomyocytes in our 3D-HO system, which are known to be susceptible to ROS stress [12,38,39].

While both the 3D-HO and 2D-CM models are effective for assessing DIC responses observed in patients, the detailed response patterns to doxorubicin differ between the two systems, particularly in the DOXTOX groups. We observed that 3D-HOs were relatively less sensitive to doxorubicin, as indicated by their higher $IC_{50}$ values, and showed different responses to apoptosis markers than 2D-CMs. The difference in responses between 2D-CMs and 3D-HOs can be influenced by the structural characteristics of 3D-HOs, cell-cell interactions, and the proportion of various cell types [7,40]. These findings suggest that the 3D-HO model requires a separate drug conditioning process compared to 2D-CMs to accurately reflect drug responses, even though 3D models effectively mimic tissue-level responses observed in patients [41].

Our study highlights the importance of choosing the appropriate model system and carefully considering the treatment method to accurately predict individual variations in drug responses. This approach could provide a foundation for future personalized treatments, offering important insights into predicting drug responses in patients. Additionally, our results suggest that the 3D-HO model could potentially complement traditional 2D-CM model. Future research should aim to confirm the broad applicability of this model across more diverse patient groups and monitor drug responses over longer periods to evaluate its practical use in clinical settings.

## Ethical statement

Human PBMC isolation and hiPSC generation were performed with informed consent from all participants and were approved by the Institutional Review Board (IRB) of the Samsung Medical Center (IRB: 2016-11-025-015) under standardized protocols. All research was performed in accordance with relevant guidelines and regulations.

## Data availability statement

All data generated in this study is available from the corresponding author (Jaecheol Lee) upon request.

## Funding

This work was supported by National Research Foundation of Korea (NRF) grants funded by the Korean government (Ministry of Science and ICT, MSIT) (2019R1C1C1010675, 2020M3A9E4037902, and 2019R1A5A2027340) and Korean Fund for Regenerative Medicine (KFRM) grants funded by the Korean government (MSIT, Ministry of Health & Welfare) (22A0302L1). This research was supported by a grant from the Korea Health Technology R&D Project through the Korea Health Industry Development Institute (KHIDI), funded by the Ministry of Health and Welfare, Republic of Korea (grant number: HR22C1363).

## CRediT authorship contribution statement

**Jiye Jang:** Methodology, Formal analysis. **Hyewon Jung:** Writing – original draft, Formal analysis. **Jaekyun Jeong:** Writing – original draft, Visualization. **Junseok Jeon:** Resources. **Kyungho Lee:** Resources. **Hye Ryoun Jang:** Supervision, Resources. **Jeung-Whan Han:** Supervision, Funding acquisition. **Jaecheol Lee:** Writing – review & editing, Validation, Supervision, Project administration, Methodology, Funding acquisition, Data curation, Conceptualization.

## Declaration of competing interest

The authors declare that they have no known competing financial interests or personal relationships that could have appeared to influence the work reported in this paper. Jaecheol Lee reports financial support was provided by National Research Foundation of Korea. Jaecheol Lee reports financial support was provided by Korea Health Industry Development Institute. Jaecheol Lee reorts financial support was provided by Korean Fund for Regenerative Medicine. If there are other authors, they declare that they have no known competing financial interests or personal relationships that could have appeared to influence the work reported in this paper.

## Acknowledgements

The DOX and DOXTOX hiPSCs were transferred from Greenstone Biosciences, Inc., a drug discovery company based in Palo Alto, California, USA (https://greenstonebio.com/). We appreciate the technical support received from Kyungyi Choi, Ji Woo Kim, and Wu Hyun Lee of the Cell and Gene Therapy Institute, Samsung Medical Center, Sungkyunkwan University School of Medicine.

## Appendix A. Supplementary data

Supplementary data to this article can be found online at https://doi.org/10.1016/j.heliyon.2024.e38714.

## References

[1] Z. Zhao, et al., Organoids, Nat. Rev. Methods Primer 2 (2022) 1–21.
[2] N. Wenningmann, M. Knapp, A. Ande, T.R. Vaidya, S. Ait-Oudhia, Insights into doxorubicin-induced cardiotoxicity: molecular mechanisms, preventive strategies, and early monitoring, Mol. Pharmacol. 96 (2019) 219–232.
[3] J. Wanga, et al., Molecular mechanisms of doxorubicin-induced cardiotoxicity: novel roles of sirtuin 1-mediated signaling pathways, Cell. Mol. Life Sci. 78 (2021) 3105–3125.
[4] M. Volkova, R. Russell, Anthracycline cardiotoxicity: prevalence, pathogenesis and treatment, Curr. Cardiol. Rev. 7 (2011) 214–220.
[5] P.W. Burridge, et al., Human induced pluripotent stem cell–derived cardiomyocytes recapitulate the predilection of breast cancer patients to doxorubicin-induced cardiotoxicity, Nat. Med. 22 (2016) 547–556.
[6] M.I.C. Planek, et al., Prediction of doxorubicin cardiotoxicity by early detection of subclinical right ventricular dysfunction, Cardio-Oncol. 6 (2020) 10.
[7] P. Nair, M. Prado, I. Perea-Gil, I. Karakikes, Concise review: precision matchmaking: induced pluripotent stem cells meet cardio-oncology, Stem Cells Transl. Med. 8 (2019) 758–767.
[8] D. Thomas, S. Shenoy, N. Sayed, Building multi-dimensional induced pluripotent stem cells-based model platforms to assess cardiotoxicity in cancer therapies, Front. Pharmacol. 12 (2021).
[9] A.R. Pinto, et al., Revisiting cardiac cellular composition, Circ. Res. 118 (2016) 400–409.
[10] F. Guo, et al., Crosstalk between cardiomyocytes and noncardiomyocytes is essential to prevent cardiomyocyte apoptosis induced by proteasome inhibition, Cell Death Dis. 11 (2020) 1–13.
[11] G. Chen, et al., Chemically defined conditions for human iPSC derivation and culture, Nat. Methods 8 (2011) 424–429.
[12] Y.R. Lewis-Israeli, et al., Self-assembling human heart organoids for the modeling of cardiac development and congenital heart disease, Nat. Commun. 12 (2021) 5142.
[13] P.W. Burridge, et al., Chemically defined generation of human cardiomyocytes, Nat. Methods 11 (2014) 855–860.
[14] P.W. Burridge, A. Holmström, J.C. Wu, Chemically defined culture and cardiomyocyte differentiation of human pluripotent stem cells, Curr. Protoc. Hum. Genet. 87 (2015), 21.3.1-21.3.15.
[15] S.M. Swain, F.S. Whaley, M.S. Ewer, Congestive heart failure in patients treated with doxorubicin, Cancer 97 (2003) 2869–2879.
[16] W.-T. Hsu, C.-Y. Huang, C.Y.T. Yen, A.-L. Cheng, P.C.H. Hsieh, The HER2 inhibitor lapatinib potentiates doxorubicin-induced cardiotoxicity through iNOS signaling, Theranostics 8 (2018) 3176–3188.

[17] N. Kumar, et al., Assessment of temporal functional changes and miRNA profiling of human iPSC-derived cardiomyocytes, Sci. Rep. 9 (2019) 13188.
[18] F. Laco, et al., Unraveling the inconsistencies of cardiac differentiation efficiency induced by the GSK3β inhibitor CHIR99021 in human pluripotent stem cells, Stem Cell Rep. 10 (2018) 1851–1866.
[19] B. Wu, H.S. Baldwin, B. Zhou, Nfatc1 directs the endocardial progenitor cells to make heart valve primordium, Trends Cardiovasc. Med. 23 (2013) 294–300.
[20] K. Ban, et al., Purification of cardiomyocytes from differentiating pluripotent stem cells using molecular beacons that target cardiomyocyte-specific mRNA, Circulation 128 (2013) 1897–1909.
[21] C. Rudat, A. Kispert, Wt1 and epicardial fate mapping, Circ. Res. 111 (2012) 165–169.
[22] B. Wu, et al., Nfatc1 coordinates valve endocardial cell lineage development required for heart valve formation, Circ. Res. 109 (2011) 183–192.
[23] T. Akamatsu, et al., Direct isolation of myofibroblasts and fibroblasts from bleomycin-injured lungs reveals their functional similarities and differences, Fibrogenesis Tissue Repair 6 (2013) 15.
[24] R.M. Barnes, B.A. Firulli, S.J. Conway, J.W. Vincentz, A.B. Firulli, Analysis of the Hand1 cell lineage reveals novel contributions to cardiovascular, neural crest, extra-embryonic, and lateral mesoderm derivatives, Dev. Dynam. 239 (2010) 3086–3097.
[25] Y. Morikawa, F. D'Autréaux, M.D. Gershon, P. Cserjesi, Hand2 determines the noradrenergic phenotype in the mouse sympathetic nervous system, Dev. Biol. 307 (2007) 114–126.
[26] F. Strutz, et al., Identification and characterization of a fibroblast marker: FSP1, J. Cell Biol. 130 (1995) 393–405.
[27] D.M. Milewicz, R.E. Pyeritz, E.S. Crawford, P.H. Byers, Marfan syndrome: defective synthesis, secretion, and extracellular matrix formation of fibrillin by cultured dermal fibroblasts, J. Clin. Invest. 89 (1992) 79–86.
[28] D.M. Milewicz, et al., A mutation in FBN1 disrupts profibrillin processing and results in isolated skeletal features of the Marfan syndrome, J. Clin. Invest. 95 (1995) 2373–2378.
[29] C.R. Archer, et al., Characterization and validation of a human 3D cardiac microtissue for the assessment of changes in cardiac pathology, Sci. Rep. 8 (2018) 10160.
[30] M. Xu, D.J. McCanna, J.G. Sivak, Use of the viability reagent PrestoBlue in comparison with alamarBlue and MTT to assess the viability of human corneal epithelial cells, J. Pharmacol. Toxicol. Methods 71 (2015) 1–7.
[31] X. Chen, et al., Assessment of doxorubicin toxicity using human cardiac organoids: a novel model for evaluating drug cardiotoxicity, Chem. Biol. Interact. 386 (2023) 110777.
[32] M.C. Wei, et al., Proapoptotic BAX and bak: a requisite gateway to mitochondrial dysfunction and death, Science 292 (2001) 727–730.
[33] T. Shibue, et al., Differential contribution of Puma and Noxa in dual regulation of p53-mediated apoptotic pathways, EMBO J. 25 (2006) 4952–4962.
[34] J. Ma, et al., High purity human-induced pluripotent stem cell-derived cardiomyocytes: electrophysiological properties of action potentials and ionic currents, Am. J. Physiol. Heart Circ. Physiol. 301 (2011) H2006–H2017.
[35] M. Clements, N. Thomas, High-throughput multi-parameter profiling of electrophysiological drug effects in human embryonic stem cell derived cardiomyocytes using multi-electrode arrays, Toxicol. Sci. 140 (2014) 445–461.
[36] H.B. Hayes, et al., Novel method for action potential measurements from intact cardiac monolayers with multiwell microelectrode array technology, Sci. Rep. 9 (2019) 11893.
[37] J.M. Dewing, V. Saunders, I. O'Kelly, D.I. Wilson, Defining cardiac cell populations and relative cellular composition of the early fetal human heart, PLoS One 17 (2022) e0259477.
[38] H. Kim, R.D. Kamm, G. Vunjak-Novakovic, J.C. Wu, Progress in multicellular human cardiac organoids for clinical applications, Cell Stem Cell 29 (2022) 503–514.
[39] B. Volmert, et al., A patterned human primitive heart organoid model generated by pluripotent stem cell self-organization, Nat. Commun. 14 (2023) 8245.
[40] I. Ribitsch, et al., Large animal models in regenerative medicine and tissue engineering: to do or not to do, Front. Bioeng. Biotechnol. 8 (2020).
[41] J.G. Moffat, F. Vincent, J.A. Lee, J. Eder, M. Prunotto, Opportunities and challenges in phenotypic drug discovery: an industry perspective, Nat. Rev. Drug Discov. 16 (2017) 531–543.